MODIFICATION OF SPANWISE STRUCTURES DUE TO THE PROXIMITY OF A SOLID WALL

Miodrag Darko Matovic
Department of Mechanical Engineering, Queen's University
Kingston, Ontario, Canada, K7L 3N6
matovic@me.queensu.ca

Robert Martinuzzi
Department of Mechanical & Materials Engineering, The University of Western Ontario
London, Ontario, Canada, N6A 5B9
rmartinu@julian.uwo.ca

ABSTRACT

The turbulent flow around a square cross-section cylinder mounted in the vicinity of a solid wall has been simulated using Large Eddy Simulation. The results are compared to velocity and pressure field measurements. The predicted flow field captures essential features observed in experiments. The existence of spanwise jitter and secondary three-dimensional flow structures, which are generally not observed using the different time dependent RANS techniques, could be reproduced reliably.

INTRODUCTION

Periodic vortex shedding past bluff bodies is of fundamental interest because of complex interaction between competing mechanisms. The coupling of opposite shear layers promotes the formation of a vortex street, the stability of which is perturbed by incoherent turbulent fluctuations. Recently, increased interest in such flows is motivated by engineering applications (*e.g.* dispersion, cooling of electronic components, wind engineering) and by advances in predictive capabilities using large eddy simulation. Much of the literature has focused on the flow around isolated or surface-mounted square cylinders. Flows around obstacles in the vicinity of the solid surface have received much less attention, although it could be argued that they occur more often in engineering practice than either of the extreme cases. The vicinity of the solid wall interferes with both aforementioned competing mechanisms, by inviscid pressure/continuity effects, through the cylinder-to-wall separation (S) and by viscous effects generated at the wall expressed through the boundary layer thickness (δ).

Durao et al (1991) and Bosch and Rodi (1996) measured the flow around a square cylinder near a wall at Re of 13,600 and 22,000, respectively. They identified the threshold gap of S/D =0.375 for the onset of vortex shedding. Martinuzzi and Wu (1997) investigated experimentally the flow in similar geometry, and found that no shedding occurs for $S/D<0.3$, that for intermediate gap heights ($0.5<S/D<2$) the presence of the obstacle results in a thickening of the wall boundary layer and that the near wake turbulent field is asymmetric. It is also observed that separation of the solid wall boundary layer is accompanied by an upwash of the wake flow.

Numerical studies of the flow past square cylinders were mostly done by unsteady RANS models or laminar flow calculations. Bosh and Rodi (1996) used the Kato and Launder (1993) modification to reduce the excessive production of k at the cylinder front face. Sohankar *et al* (1999) performed direct numerical simulations of low Re number flows around the square cylinder (up to Re=500) and found a Strouhal number increase of the order of 20% when the calculation were performed in 3D (as opposed to 2D planar geometry), with the cylinder span of 6 diameters. These studies indicate that a full three-dimensional simulation is necessary to capture the fundamental physical processes even though the flow is two-dimensional in the mean.

The existence of three-dimensional coherent structures in mean two-dimensional wakes has been shown to exist both experimentally and numerically. For example, at moderate to high Reynolds numbers, the laminar wake of a circular cylinder is characterized by the quasi-periodic passage of Von Karman vortices (rollers). Spanwise variation of the rollers' shedding phase can result in three shedding patterns: normal, oblique or chevron. The regularity of these patterns is disturbed by the presence of two types of secondary, spanwise instabilities, which can trigger a change of mode (Williamson, 1996). For turbulent flows, the existence of secondary spanwise structures (ribs) at roughly half the frequency of the rollers has been inferred from multi-point anemometry and pattern recognition techniques (Perry *et al.*, 1982; Kiya and Matsamura, 1988). Direct experimental evidence in turbulent flows is difficult due to the inherent limitations of Eulerian-based anemometry techniques in quantifying

transient flow structures. It is thus an increasingly accepted practice to extract structure information from numerical simulations subject to direct experimental validation.

To our best knowledge this is the first reported LES study of the flow past a square cylinder in the vicinity of a solid wall. The aim of the study is to examine whether LES data can provide sufficient additional insight into the spanwise structure topology, their modification by the presence of the solid wall and to reveal the mechanism(s) of spanwise jitter observed in the pressure time series recorded at the cylinder surface.

EXPERIMENTAL SETUP AND MEASUREMENT TECHNIQUES

The experiments were conducted in a suction-type, open-circuit subsonic wind-tunnel with settling chamber to test section contraction of 6:1. The geometry and nomenclature are summarized in Fig. 1. Air is drawn at the inlet through a fine meshed screen grid and a honeycomb flow straightener. The test section is a 0.457 m (18") square. The test model, a square cylinder made of steel to ensure sharp edges, is placed midway into the working section, 40D downstream of the test section entrance, with one face perpendicular to the oncoming flow. The square cylinder side dimensions are D = 0.0254 m (1") and the span is 18D. A smooth flat plate with a serrated leading edge and adjustable end flap was used to obtain a controlled, fully-turbulent boundary

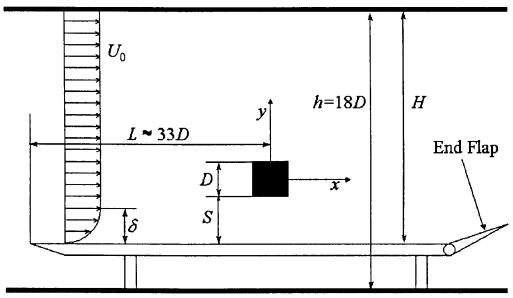

Figure 1: The wind tunnel flow geometry

layer. The square prism was placed at L = 33D downstream of the plate leading edge. The boundary layer thickness, measured in the absence of the obstacle was δ = 1.5D at the cylinder leading edge position.

Velocity measurements were performed by a two-component Laser Doppler Velocimetry (LDV) system and by Hot-Wire Anemometry (HWA, for which even time sampling was used). The details of measurement technique are given by Martinuzzi and Wu (1997).

NUMERICAL METHOD

The set of incompressible flow equations solved are:

$$u_{i,i} = 0\,, \tag{1}$$

$$\left(\rho u_i\right)_{,t} + \left(\rho u_i u_j\right)_{,j} = -p_{,i} + \left(2\mu S_{ij}\right)_{,j} - \tau_{ij,j}\,, \tag{2}$$

where S_{ij} is the strain rate tensor, τ_{ij} is the residual (subgrid) shear stress and comma indicates a derivative. The pre-filtering operation in the present calculations is done implicitly (i.e. the grid size serves as a spatial filter, Ciofalo, 1994), thus the unresolved subgrid terms contain only subgrid velocity correlations

$$\tau_{ij} = \rho\widehat{u'_i u'_j}\,, \tag{3}$$

where the primes indicate subgrid fluctuating components and an arched overbar indicates spatial averaging at the subgrid scale. In this study a Smagorinsky subgrid scale model was used:

$$\tau_{ij} = -2\mu_s S_{ij}\,, \tag{4}$$

where the subgrid viscosity is modelled as

$$\mu_s = \rho\left(C_s\Delta\right)^2\left(2S_{ij}S_{ij}\right)^{1/2}. \tag{5}$$

The Smagorinsky constant C_s was taken as 0.1, following recommendations of Piomelli *et al* (1989). The subgrid filter size, Δ was calculated from

$$\Delta = \left(\left(\Delta_1^2 + \Delta_2^2 + \Delta_3^2\right)/3\right)^{1/2} \tag{6}$$

as suggested by Bardina *et al.* (1980) for anisotropic meshes, where Δ_i are cell volume sizes in three (curvilinear) coordinate directions. More complex subgrid models, such as the one-equation model of Davidson (1997) are also good candidates for this type of flow (Sohankar, 2000). The governing equations were solved by a finite volume, multi-block in-house developed code FLEX, using a blend of 80% third order scheme (SMART) and 20% upwind differencing (Ferziger and Peric, 1996). Pressure-velocity coupling was handled by a collocated scheme of Rhie and Chow (1983).

The computational domain was chosen to closely resemble the experimental conditions described in the previous section. The domain is shown schematically in Fig. 2. It is composed of five blocks, four of which are clustered around the square cylinder and the fifth covering the upper portion of the flow domain.

The near-field around the cylinder surface is resolved by a highly stretched grid with the first grid node at 0.0005*D* away from the cylinder surface, and stretching up to 0.06D at the end of the domain. The close-up of the grid around the square cylinder is shown in figure 3. Dense grid lines run almost

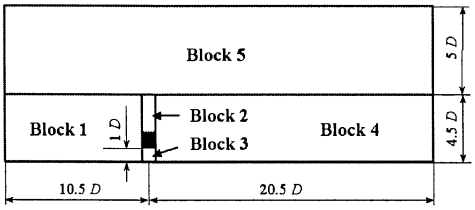

Figure 2: Multi-block computational domain

parallel to the solid surface, but these gradually fan out into the uniform mesh at the exit boundary, except the clustering near the wall, which is

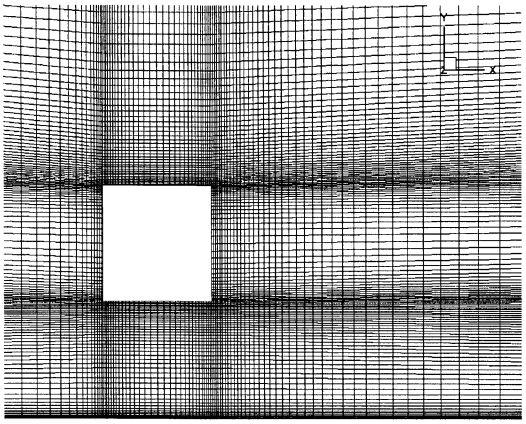

Figure 3: Computational mesh close-up around the square cylinder.

maintained. By employing this type of node distribution the grid is nearly orthogonal everywhere, but the excessive cell aspect ratios near the domain edges, typical for this type of flow domains (essentially square "C" grids), are avoided.

Boundary conditions were specified 10*D* upstream of the cylinder leading edge as: a steady, fixed velocity inlet with the boundary layer thickness of $\delta=D$ over the solid wall. The two side walls (z=0 and $z=B$) and the far parallel wall (y=H) are modelled as slip (symmetry) boundaries. The outlet was set as an outflow boundary with zero velocity gradients. The non-dimensional time step (physical time multiplied by U_0/D) was held at Δt=0.05 .

PRESENTATION AND DISCUSSION OF RESULTS

The experimental and numerical vector plots of the mean velocity field are shown in Fig. 4. The experimental results were obtained by averaging 30,000 LDV signals at each point. The numerical results were obtained by averaging 1,700

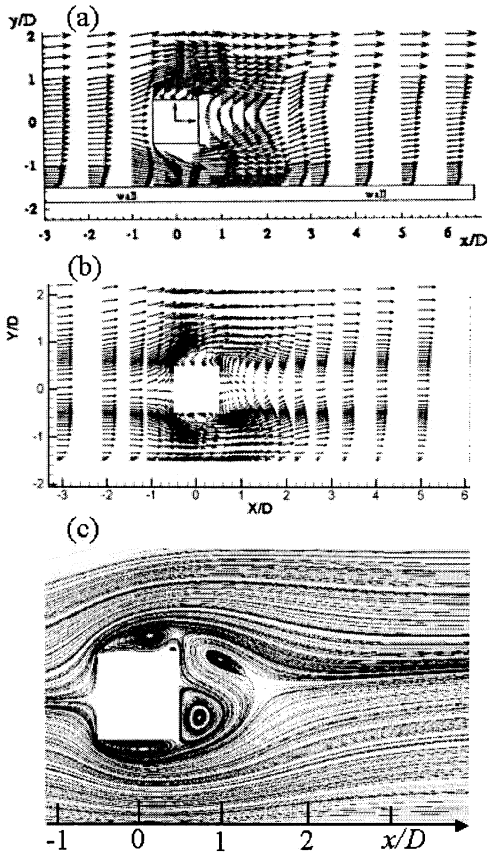

Figure 4. Mean velocity field in a *xy* plane: (a) experimental data; (b) LES mean field; (c) LES mean streamtraces.

instantaneous snapshots spanning over 60 cycles. The case compared here is for the gap size $S=D$, both experimentally and computationally. The Strouhal number ($St=fD/U_\infty$) in the experimental study was 0.134 which is close to the numerical simulations value of 0.138.

Very good agreement between the experimental and numerical flow field is clear from the vector plots in the vicinity of the obstacle. The position of a saddle point behind the cylinder is one diameter behind the trailing edge (x/D=1.5). Based on this agreement, further insights into the flow topology can be drawn by decomposing the velocity (and pressure) field into the mean, periodic and

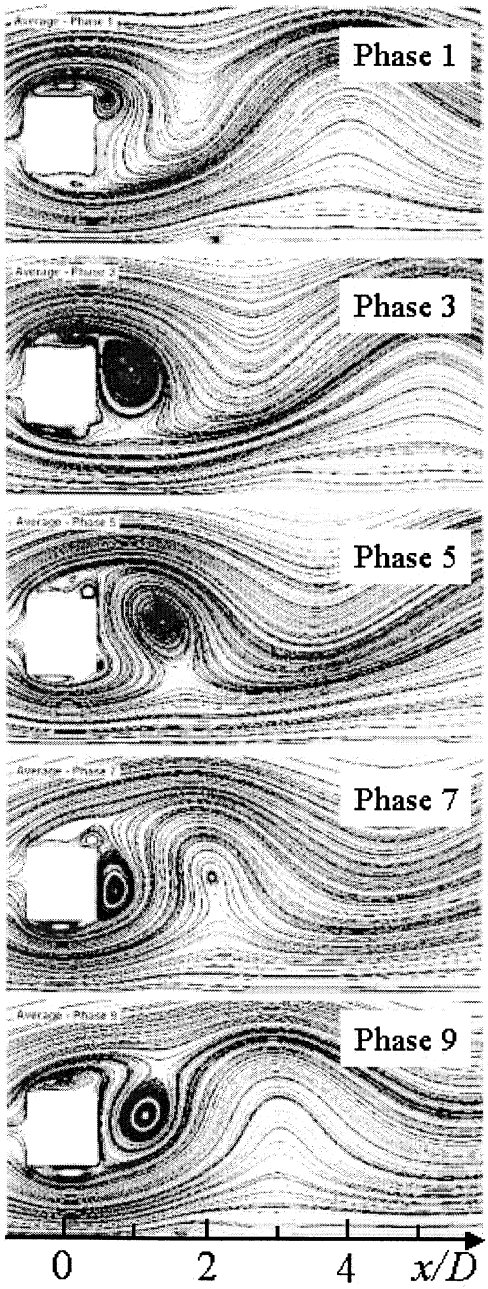

Figure 5: Phase averages of instantaneous streamtraces in the vicinity of a square cylinder. Each frame is an average of 170 snapshots over 60 cycles

fluctuating components (Bosh and Rodi, 1998):

$$\phi(t) = \overline{\phi} + \tilde{\phi}(t) + \phi' = \langle \phi \rangle(t) + \phi' \,, \qquad (7)$$

where $\langle \phi \rangle(t)$ is the ensemble (phase) averaged variable field. In practical evaluations, the questions of reference signal for phase averaging and the phase duration used in averaging naturally arises. Several flow variables could be used for this purpose: pressure at some reference point, spanwise pressure average, u or v velocity at some characteristic point, etc. Thus the choice of reference phase information is not unique. In this study the pressure at the centre of the top cylinder surface (streamwise and spanwise) was selected for two reasons: pressure is generally better indicator of the global phase

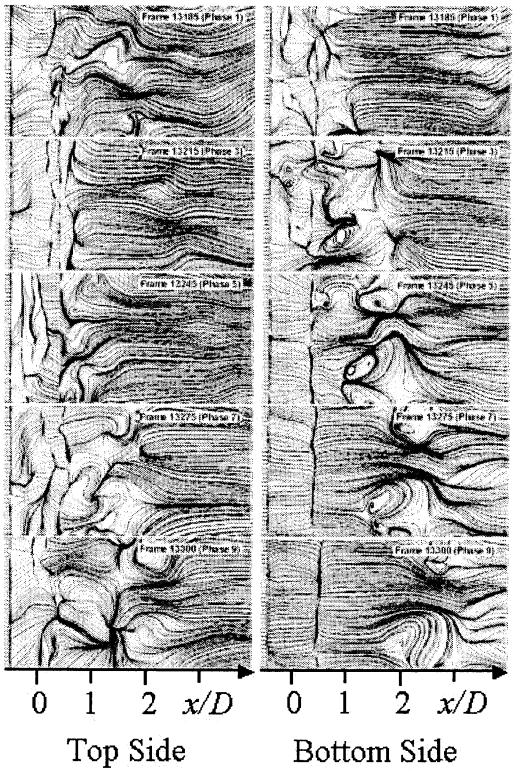

Figure 6: Instantaneous streamtrace snapshots spanning one shedding cycle. XZ planes just above (left) and below (right) the square cylinder. The frames correspond to phases 1 3 5 7 and 9.

information (being a fully elliptic variable), and the value at the cylinder surface is easy to monitor experimentally. The duration of each cycle was determined individually as the time elapsed between two reference pressure peaks (interpolated value), then divided into 10 phase bins. Tests of other pressure locations showed that the pressure time series at the cylinder front and bottom are of similar quality, while the pressure on the lee is too noisy.

The temporal sequence of vortex shedding, as influenced by the proximity to the wall can be followed through the phases. At the beginning of the shedding cycle, the wake region behind the cylinder is filled by the growing vortex spilling out from the

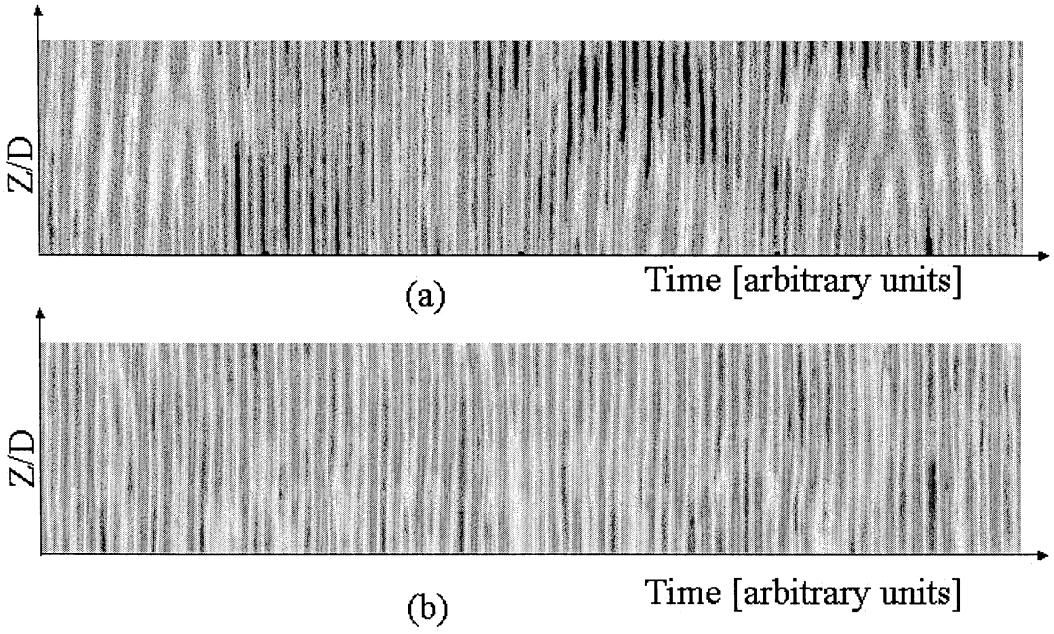

Figure 7: Time sequence of pressure magnitude along the top centre of the square cylinder. (a) experimental data. (b) LES simulations. Span is 4.5 diameters in both cases.

top edge (phases 1 to 3) until it detaches (phase 5) and the growth starts from the lower edge. Note that the top side of the cylinder houses two vortices most of the time, while the bottom one has only one, thinner vortex, due to the wall proximity, consistent with the average field in Fig. 4. Also, the detached top vortex is larger than the bottom one and the upsweep of the wake by the faster stream near the wall is evident.

To assess the extent of three-dimensionality of the flow structures the spanwise features of the flow are considered. The computational domain spans 8 diameters, represented by 33 uniform finite volumes in Z direction. The phase averages of XZ plane view did not reveal significant features, indicating a lack of coherence between the spanwise and the streamwise structures.

Kiya and Matsumura (1988) observed a similar lack of coherence for the flow behind a flat plate mounted normal to the on-coming flow. They argued that while the inception of these structures was related to three-dimensional instabilities of the rollers, the occurrence was randomly distributed in space.

To extract the typical spanwise features we can either rely on instantaneous fields or employ conditional sampling essentially adapting the phase averaging paradigm to the randomly occurring flow structures. Only the first approach is taken here, the latter being planned for future work.

In Fig. 6. five pairs of instantaneous streamtrace snapshots are shown, depicting the spanwise eddies in the planes 0.04D above the top cylinder surface or 0.04D below the bottom cylinder face.

The surface topology of these features is consistent with the "ribs" observed by Kiya and Matsumura (1988). Counter rotating pairs normal to the streamwise direction appear, which are sectional cuts through a closed structure occurring between rollers. While a characteristic length can be assigned to these structures, there spanwise occurrence is randomly distributed.

The strong bending of streamtraces in the spanwise direction indicates very strong lateral movement of fluid particles. The maximum velocity magnitude in z direction was monitored during the calculations and was typically close to the average streamwise velocity. This is consistent with vigorous displacement of fluid particles by the spanwise structures indicated in the instantaneous snapshots. If there were no wall close to the cylinder there should be skew symmetry between the planes above and below the cylinder, i.e. the phase 1 to the left should be similar to the phase 5 to the right (more precisely, to the phase 6, but only odd phases are shown here), etc. Comparison of the two columns indicates here that the similarity does exist between phases 7 and 9 above the cylinder with phases 1 and 3 below, thus pointing to the similar topology of one half of the shedding cycle. The process of recirculation bubble growth is similar for the top and the bottom part, but the sweep half-cycle occurring at the near-wall side of the cylinder is distorted by the presence of the wall. The sweep

phases from above (phases 1 and 3 at the top) are less vigorous, thus the spanwise structures remain attached to the lee side of the cylinder. Contrary to that, the sweep half-cycle from below is faster, resulting in much better alignment of the streamlines with the main flow direction, the intense spanwise structures being swept full cylinder diameter behind the lee side.

The extent of spanwise phase jitter is illustrated in Fig. 7 by the pressure level time sequences recorded along the top side of the square cylinder. The overall magnitude of the jitter is very similar in experimental and in computational cases, but the there is the qualitative difference between the two sequences. There is experimental evidence of cycle bifurcation indicating that two rollers have merged, leading to a loss of a shedding cycle along the part of the surface of the cylinder. Also, there are clear periods of time for which the pressure signal is much stronger over certain areas. These two observations would be consistent with the existence and the influence of three-dimensional instabilities. However, the location of these events seems to vary randomly in the spanwise direction, and are thus difficult to capture with conventional anemometry. Cycle skip was not observed in the LES simulations analysed here.

CONCLUSIONS

The preliminary results of an LES simulation for the turbulent flow around a square cylinder in the proximity of a solid wall were presented for a cylinder-to-wall separation of $S/D = 1$. The study was motivated by the observation that even three-dimensional implementations of phased-averaged single-point closure schemes (RANS) failed to capture some of the important flow features observed experimentally. Of particular interest were: the existence of spanwise phase-jitter and the existence of secondary coherent structures due to three-dimensional instabilities.

The predicted and experimentally measured mean flow field agreed very well. The simulation was able to capture the shedding frequency to within experimental uncertainty. More significantly, the spanwise phase-jitter observed experimentally was well captured in the LES simulation. The predicted flow field also allowed for the detection of three-dimensional structures. The simulated behaviour matched closely that observed experimentally. However, the cycle-skip, which has been associated with vortex dislocation for rollers in laminar flows (Williams, 1996) and is observed experimentally, could not be detected in the simulations.

The present study is now the subject of further investigations, for which different conditional sampling techniques and vortex recognition algorithms will be employed to complement the existing experimental results.

References

S.C.C. Bailey, "Experimental Investigation of the Pressure Distribution for a Square Cylinder near a Solid Boundary", M.E.Sc. Thesis, The University of Western Ontario (2001).

Bosh, G. and Rodi, W., "Simulation of Vortex Shedding Past a Square Cylinder near a Wall", *Int. J. Heat and Fluid Flow*, **17**:267–275 (1996).

Bosh, G. and Rodi, W., "Simulation of Vortex Shedding Past a Square Cylinder with Different Turbulence Models", *Int. J. Num. Meth. Fluids*, **28**:601–616 (1998).

Durao, D. F. G., Gouveia, P. S. T. and Pereira, J. C. F., "Velocity characteristics of the flow around a square cross section cylinder placed near a channel wall", *Exp. in Fluids,* 11:341-350 (1991).

Kiya, M. and Matsumura, M., "Incoherent Turbulence Structure in the Near Wake of a Square Cylinder: a Guide to the Data." *JFM*, **190**:343–356 (1988).

Martinuzzi, R. J. and Wu, K. C. Q., "An experimental investigation of the flow around a two-dimensional square prism in the proximity of a solid wall: effect of the gap size", *11th Int. Symp. on Turb. Shear Flows,* Grenoble, France (1997).

Perry, A. E., Chong, M. S and Lim, T. T., "The vortex-shedding process behind two-dimensional bluff bodies", *JFM*, **116**:77-90 (1982).

Sohankar, A., Norberg, C. and Davidson, L., "Simulation of Three-dimensional Flow a Square Cylinder at Moderate Reynolds Numbers", *Phys. Fluids*, **11**(2):288–306 (1999)

Williamson, C.H.K, "Vortex Dynamics in the Cylinder Wake", *Ann. Rev. Fluid Mech*, **28**:477–539 (1996)